Texas A&M University
Mechanical Engineering Department
Turbomachinery Laboratory
Tribology Group

MEASUREMENT OF LEAKAGE AND ESTIMATION OF FORCE COEFFICIENTS IN A SHORT LENGTH ANNULAR SEAL SUPPLIED WITH A LIQUID/GAS MIXTURE (STATIONARY JOURNAL)

TRC-SEAL-01-15

Research Progress Report to the Turbomachinery Research Consortium

by
Luis San Andrés
Mast-Childs Chair Professor
Principal Investigator

Xueliang Lu, Qing Liu
Research Assistants

May 2015

WET SEALS FOR SUB-SEA MULTIPLE PHASE COMPRESSORS

TRC Project, TEES # 32513/1519NS

EXECUTIVE SUMMARY

Luis San Andrés

In the oil and gas industry, compressors and pumps may operate under two phase or even multiple phase flow conditions, i.e., liquid in gas for compressors and gas in liquid for pumps. In the near future, subsea factory compressors must handle, without significant efficiency and power penalty, a two phase flow with a liquid volume fraction as high as 5%. Off-design operation affects system overall efficiency and reliability, including penalties in leakage and rotordynamic performance of secondary flow components, namely seals. Besides the seminal paper of Iwatsubo and Nishino (1993) for a pump seal, there is no test data for the force coefficients of seals operating with either liquid in gas or a gas in liquid condition.

The report describes measurements of leakage and force coefficients conducted in the TRC vertical test rig holding a short length (L/D = 0.36) smooth annular seal with clearance (c)=0.127 mm (D=127mm), and operating with a liquid in a gas mixture. The test rig has a transparent seal cartridge supported atop one pipe, as well as a journal, rigidly supported on two ball bearings. A sparger element installed upstream of the seal inlet, mixes ISO VG 10 oil and dry air at a room temperature (20 ºC) and continuously supplies oil-gas mixtures with a steady liquid volume fraction (LVF) to the seal.

In tests conducted with a stationary (non-rotating) journal and with a supply pressure P_S=3.5 bar(abs), the mass flow rate, increases rapidly as the inlet LVF increases from 0.04 to 0.2. Since the liquid mass fraction ~1 for LVF>0.30, the growth in mass flow reduces as the LVF raises towards an all liquid condition (LVF=1). The large difference in density between the liquid (oil) and gas (air) determines that the liquid mass content in the mixture be rather large even when the LVF is just at a low percentage.

(Single frequency) dynamic load excitations exerted on the test seal produced system motions from which to determine dynamic force coefficients for operation with a pressure supply/pressure discharge ratio =2.0 and operating with air (only) and also with an oil in air mixture with inlet LVF=2% and 4%. The experimental results, first of its kind, reveal a small amount of liquid increases ten-fold (or more) the damping coefficients of the *wet* seal. Damping coefficients attained for operating conditions with a small volume fraction of oil in gas (4%) can be twenty times larger than those obtained for the pure gas condition. The effect of a few *droplets* of liquid on affecting the test system forced response is overwhelming.

TABLE OF CONTENTS

EXECUTIVE SUMMARY I
INTRODUCTION 1
LITERATURE REVIEW 1
TEST RIG DESCRIPTION 4
FLOW RATE THROUGH SEAL 8
PERIODIC FORCED RESPONSE OF TEST SEAL AND ESTIMATION OF FORCE COEFFICIENTS 11
Unidirectional Periodic Load Tests on *Dry* Structure 12
Force Coefficients for Seal Operating With Liquid in Gas Mixture 13
CONCLUSION 18
REFERENCES 19
Appendix A. Formulas for the Viscosity of a Mixture 21
Appendix B. Uncertainly analysis 23
Appendix C. Real and Imaginary Part of Cross-Coupled Stiffness (H_{XY} and H_{YX}) for *Wet Seal* 27
Appendix D. Oil Viscosity Measurement 28

LIST OF TABLES

Table 1. Annular wet seal dimensions and fluids parameters 5
Table 2. Formulars for evaluation of the effective viscosity of a (gas in liquid) mixture 7
Table 3. Measured weight and estimated effective mass of the test seal system 11
Table 4. Test system structural force coefficients. 12
Table 5. Direct stiffness and mass coefficients for *wet s*eal supplied with oil in gas mixture. Tests with supply pressure P_S=2.0 bar (abs), ambient pressure P_a=1 bar (abs), inlet temperature 20^{o}C. Stationary (non-rotating) journal [13] 16
Table A.1. Mixture viscosity models for gas-liquid mixture 21
Table B.1. Uncertainty in flow rate and pressure measurements. 24
Table B.2. Uncertainty of seal inlet GVF and mixture mass flow rate. Test with Ps=3.5bar(a), Pa=1.0 bar(a), temperature ~20°C, stationary rotor. 24
Table B.3. Uncertainties of estimated parameters for the two-phase flow smooth annular seal 26
Table D.1 Oil viscosity measurement 28

LIST OF FIGURES

Figure 1. Schematic views of the wet seal test rig [13]. 4
Figure 2. Wet seal test photograph. 5
Figure 3. Measured mass flow rate (m_m) through seal vs. P_r, seal supply/discharge pressure ratio. Pure oil. Test with inlet temperature 21℃~23℃. Stationary (non-rotating) journal. 8
Figure 4. Measured mass flow rate (m_m) through seal vs. β_{inlet}, the LVF at the seal inlet. Test with inlet temperature 20℃~22℃. Stationary (non-rotating) journal. 9
Figure 5. Liquid mass fraction (λ), through seal vs. β_{inlet}, the LVF at the seal inlet. Test with inlet temperature 20℃~22℃. Stationary (non-rotating) journal. 10
Figure 6. Mixture Reynolds number at seal inlet/exit vs , P_s/P_a = 3.5, inlet temperature 20℃~22℃. Stationary (non-rotating) journal. 11
Figure 7. Seal cartridge displacement vs. applied load 12
Figure 8. (a)Wet seal test rig with mixture, (b) An upward force applied to seal cartridge. 14
Figure 9. Schematic view of idealized two degree of freedom structure-seal system for seal force coefficient identification [20] 15
Figure 10. Real and imaginary parts of complex stiffnesses (H_{XX}, H_{YY}) for wet seal supplied with an oil in air mixture with inlet LVF (a) 0% (all gas), (b) 2%, and (c) 4%. Stationary (non-rotating) journal. Tests with supply pressure P_S=2.0 bar(abs), ambient pressure P_a=1 bar(abs), inlet temperature 20^{o}C [13]. 17
Figure 11. Direct damping coefficients $(C_{XX}, C_{YY})_{seal}$ versus excitation frequency for wet seal supplied with oil in gas mixture with inlet LVF: 0% (all gas), 2%, and 4%. Stationary (non-rotating) journal. Tests with supply pressure P_S=2.0 bar(abs), ambient pressure P_a=1 bar(abs), inlet temperature 20^{o}C[13]. 18
Figure C.1. Real and imaginary parts of cross-coupled complex stiffnesses (H_{XY}, H_{YX}) for wet seal supplied with an oil in air mixture with inlet LVF (a) 0% (all gas), (b) 2%, and (c) 4%. Stationary (non-rotating) journal. Tests with supply pressure P_S=2.0 bar(abs), ambient pressure P_a=1 bar(abs), inlet temperature 20^{o}C. 27
Figure D.1. Measured lubricant viscosity versus temperature. 28

NOMENCLATURE

c	Seal radial clearance [m]
D	Journal diameter [m]
$F_{i(t)}$	External excitation force, $i = X, Y$ [N]
L	Seal length [mm]
m_m	Mass flow rate of two-phase mixture, $m_m = m_l + m_g$ [kg/s]
m_l, m_g	Mass flow rate for pure liquid and pure gas [kg/s]
P_a, P_s	Ambient pressure and supply pressures [Pa]
p_r	Dimensionless seal pressure ratio, $p_r = P_s / P_a$ [-]
Q_m	Flow rate for two-phase mixture [m^3/s]
Q_l , Q_g	Flow rate for pure liquid and gas [m^3/s]
Re	$\mathrm{Re} = \frac{\rho_m V_z c}{\mu_m} = \frac{m_m}{\pi D \mu_m}$, seal axial Reynolds number [-]
T	Temperature [K]
V_z	Bulk flow axial velocity [m/s]
X,Y	Seal cartridge displacements [m]
x	gas mass fraction [-]
α_m	gas volume fraction [-]
β	liquid volume fraction [-]
ξ	Test rig structural damping ratio [-]
ΔP	P_s-P_a. Pressure difference [Pa]
λ	Liquid mass fraction [-]
μ_l , μ_{ga}	Liquid and as dynamic viscosity at ambient pressure [Pa.s]
μ_m	Two-phase flow effective viscosity [Pa.s]
ρ_l, ρ_{ga}	Liquid Gas density at ambient pressure [kg/m^3]
ρ_m	Mixture or two-phase fluid density [kg/m^3]
ω	External load excitation frequency [Hz]
ω_r	Frequency ratio, $\omega_r = \omega/\omega_n$ [-]
ω_n	System natural frequency [Hz]

Matrices

$\mathbf{C}$	System damping matrix, $\mathbf{C} = \mathbf{C_S} + \mathbf{C_{seal}}$ [N-s/m]
$\mathbf{C_S}$, $\mathbf{C_{seal}}$	Structure damping and seal damping matrices [N-s/m]
$\mathbf{F}$	External excitation force vector [N]
$\mathbf{H}$	$\mathbf{K}$- ω^2 $\mathbf{M}$ + i ω $\mathbf{C}$. System complex stiffness matrix [N/m]
$\mathbf{K}$	System stiffness matrix, $\mathbf{K} = \mathbf{K_S} + \mathbf{K_{seal}}$ [N/m]
$\mathbf{K_S}$, $\mathbf{K_{seal}}$	Structure and seal stiffness matrices [N/m]
$\mathbf{M}$	System mass matrix, $\mathbf{M} = \mathbf{M_{SC}} + \mathbf{M_{seal}}$ [kg]
$\mathbf{M_{SC}}$, $\mathbf{M_{seal}}$	Structure and seal mass matrices [kg]
$\mathbf{Z}$	Seal displacement vector, relative to the static journal [m]

Subscripts

a	ambient
m	Mixture or two phase flow
g	Gas
l	Liquid

Abbreviations

GVF	Gas volume fraction
LVF	Liquid volume fraction
SSV	Sub-synchronous vibration

INTRODUCTION

In the oil and gas industry, pumps and compressors sometimes operate under two- or even multiple-phase flow conditions with a mixture of oil, water, gas, and even sand. Pumps may work off-design with gas bubbles in the process liquid, and compressors work with liquid droplets in the process gas. A two-phase operating condition affects the performance and reliability of mechanical elements, including seals and bearings. Little is known about seals operating with a liquid-gas two-phase flow, except that mixtures influence its leakage rate, drag torque and dynamic force coefficients.

San Andrés [1] reviews the literature pertinent to the two-phase flow in annular seals and squeeze film dampers, reports one instance of experimental force coefficients for a pump seals published in the early 1990s, and develops a modified bulk-flow model to predict the leakage rate, power loss, and dynamic force coefficients of textured annular seals operating with homogeneous gas-liquid mixtures. Predictions for an annular seal (L/D=0.75) operating with a mixture of N_2 and ISO VG 2 oil show that an increase in the gas volume fraction leads to a steady decrease in power loss and mass flow rate. However, a dip in power loss and leakage rate happens at a low gas volume fraction (<0.3), mainly a feature of the viscosity model used for the mixture. The predicted dynamic force coefficients of a seal operating with a gas-liquid mixture depend on the excitation frequency. For most mixtures, the seal direct stiffness decreases with an increase in the excitation frequency. However, some gas volume fractions, 0.1 in [1], lead to stiffness hardening as the excitation frequency increases. The predictions in Ref. [1] are relevant to the particular seal analyzed; whether the same performance applies to other seal types or operating condition is unknown.

Most research on *wet* (bubbly) seals is theoretical; few published papers focus on experiments. The current research aims to bridge the gap by conducting dynamic load tests on an annular seal operating with an oil in air mixture and to estimate its rotordynamic force coefficients and the effect on rotordynamic stability.

LITERATURE REVIEW

Centrifugal compressors are designed to process pure gases and pumps to operate with pure liquids. Alas, in the oil and gas industry, compressors and pumps sometimes operate under two-phase or even multiphase flow conditions. For example, compressors in subsea factories must handle a two-phase flow with a liquid volume fraction (LVF) ranging from 0 to 3% [2-4]. Operation with a high surface speed and with a large pressure difference makes seals -long ones as in balance pistons- to produce large dynamic reaction forces that affect the rotordynamics of a turbomachine. In 2014, Vannini *et al*. [2] report a severe 45% sub-synchronous vibration (SSV) in a single-stage centrifugal compressor, operating with a *wet* gas whose inlet (LVF) reached 3%. The

authors believe the liquid trapped in the labyrinth seal caused the SSV, whose onset and persistence appeared with a LVF as low as 0.5%. Therefore, quantifying the effect of two-phase flow on seal performance is important. This literature review introduces some of the previous investigations in two-phase flow seals.

In 1987, Beatty and Hughes [5] introduces a turbulent flow model to predict leakage for concentric, smooth surface, annular seals working with a homogeneous two-phase flow (caused by a material phase change). The authors characterized the flow as liquid, liquid-vapor, and vapor. The liquid changes to vapor as it flows through the seal because of a decreasing pressure (expansion) and increasing enthalpy due to both shear flow energy dissipation and extrusion work. An all liquid flow entering the seal gives a higher leakage than when flowing as a two-phase flow. The authors conclude that sub-cooling of the liquid before its ingress to the seal reduces its liquid vaporization and therefore increases the mass leakage.

In 1990, Beatty and Hughes [6] present another model for turbulent two-phase flow in annular seals based on the stratified flow of the boiling liquid and vapor phases. In the model, each phase flows as a distinct, separate stream. This phenomenon may occur in seals operating at a large rotational speed, as centrifugal inertia effects sling the liquid phase outward to the stationary surface of the seal, separating it from the vapor phase. Predictions for leakage with a stratified flow model are usually slightly greater than or equal to the leakage predicted by a homogeneous equilibrium two-phase flow model.

In 1993, Iwatsubo and Nishino [7] conduct dynamic load experiments to identify the static and dynamic force characteristics of a pump annular seal with a gas in water (two-phase) flow and with a shaft rotational speed ranging from 500 rpm to 3,500 rpm. The gas in liquid (GVF) fraction ranged from 0 (no gas) to 0.7. The seal diameter equals 70 mm, its length is 70 mm, and its radial clearance is 0.5 mm. The test force coefficients decrease steadily as the gas volume fraction (GVF) increases; and, system random vibrations, due to the two-phase flow, became very large as the GVF $\rightarrow$ 1.

In 1997, Arauz and San Andrés [8] present a bulk-flow model for a cryogenic fluid damper seal undergoing a phase change, from liquid to vapor. The authors assume a continuous vaporization model having a liquid-vapor region with a homogeneous mixture. Predictions in Ref. [9], based on the bulk-flow model in Ref. [8], reveal that the seal will have a raise in direct stiffness and a drop in cross-coupled stiffness due to the large changes in fluid compressibility as it goes from a liquid to a low quality mixture over a short spatial length.

In 1999, Oike *et al*. [10] present experimental results on a floating ring seal working with liquid-vapor mixtures of Nitrogen. In the tests, at a mean temperature T_0 = 80~98 K in the seal upstream plenum, a pressure difference of ΔP = 1.25 MPa, and at a rotor speed of 0~40 krpm, the observed two-phase flow seems homogeneous. The authors study the effect of a two-phase flow area A_2 (ratio of land length operating with two-

phase flow L_2 /seal physical land length L, $A_2 = L_2 / L$) on the seal leakage. The two-phase flow area A_2 increases with shaft rotational speed. With the ΔP noted and a low T_0, the ratio of leakages, Q/Q_l, with Q as the measured leakage under two-phase flow, increases as the shaft speed increases. Unlike the flow described in Ref. [6], the Oike *et al*'s seal *sees* no transition from a homogeneous flow to a stratified flow for shaft speeds as high as 40 kprm.

In 2009, Arghir *et* al.[11] predict the rotordynamic force coefficients of textured annular seals operating with a liquid and gas (bubbly) mixture. The authors note that the presence of a non-dissolved gas in the liquid renders frequency dependent force coefficients, in particular for mixtures with GVF > 5%. Typically, except for direct damping, all the force coefficients decrease with an increase in excitation frequency.

In 2012, San Andrés [1] introduces a bulk-flow model for analysis of homogeneous two-phase flow in annular damper seals. For a seal with diameter (D) = 116.8 mm, length (L) = 87.6 mm, radial clearance (c) = 126.7 μm, and operating at ΔP = 70 bar with N_2/ISO VG2 oil; the leakage and power loss steadily decrease as the GVF→ 1. Cross-coupled stiffnesses and direct damping decrease steadily with an increase of the GVF at the seal inlet. The excitation frequency has a pronounce effect on the seal rotordynamic force coefficients.

The most recent experiment results by San Andrés *et al*. in 2015 [12] for a short length (L/D = 0.36), smooth surface annular seal with a stationary shaft operating with a ISO VG10 oil in air mixture, shows that the mass leakage increase rapidly as the inlet LVF increases. The authors conduct experiments to estimate the seal dynamic force coefficients for operation with an oil in air mixture of LVF equal to 0.02 and 0.04 at the seal inlet plane. The parameter estimation procedure shows that the seal direct stiffness, damping and fluid inertia coefficients increase steadily as the liquid volume faction increases. Most notably, the seal direct damping increases ~20 times when the oil LVF raises s from 0 (pure gas) to just 4%.

TEST RIG DESCRIPTION

Figure 1 shows a schematic view of the *wet seal* test rig composed of a seal cartridge and a rigid shaft. The vertical rig has a transparent seal cartridge supported by a pipe and a stationary journal, rigidly supported by two ball bearings. Table 1 lists the seal dimensions as well as the lubricant characteristics. The smooth surface annular seal has a diameter (D) of 127mm, an axial length (L) equal to 46mm, and a radial clearance (c) of 0.127mm. Figure 2 depicts a photograph of the test rig with a sparger element mixing streams of ISO VG 10 oil with dry air. Both the oil and the compressed (dry) air mix at an ambient temperature (~20ºC). At the supply temperature of 20ºC, the oil viscosity (μ_l) is ~18cP and its density (ρ_l) is 830kg/m^3. An air mass flow meter and an oil turbine flow meter installed upstream of the sparger element measure the volumetric flow rates of both the gas and the oil. The transparent polycarbonate seal cartridge makes the mixture flow easily observable.

Two orthogonally (softly) mounted electromagnetic shakers excite, via two long stingers, the test seal cartridge with a periodic load with frequency 30Hz to 200Hz, in steps of 10 HZ. Two load cells connected to the seal housing measure the excitation forces. Two eddy current sensors and two piezoelectric accelerometers record the test seal motions and accelerations along two orthogonal directions (X & Y direction). During operation an oscilloscope displays the cartridge motion detected by two eddy current proximity sensors.

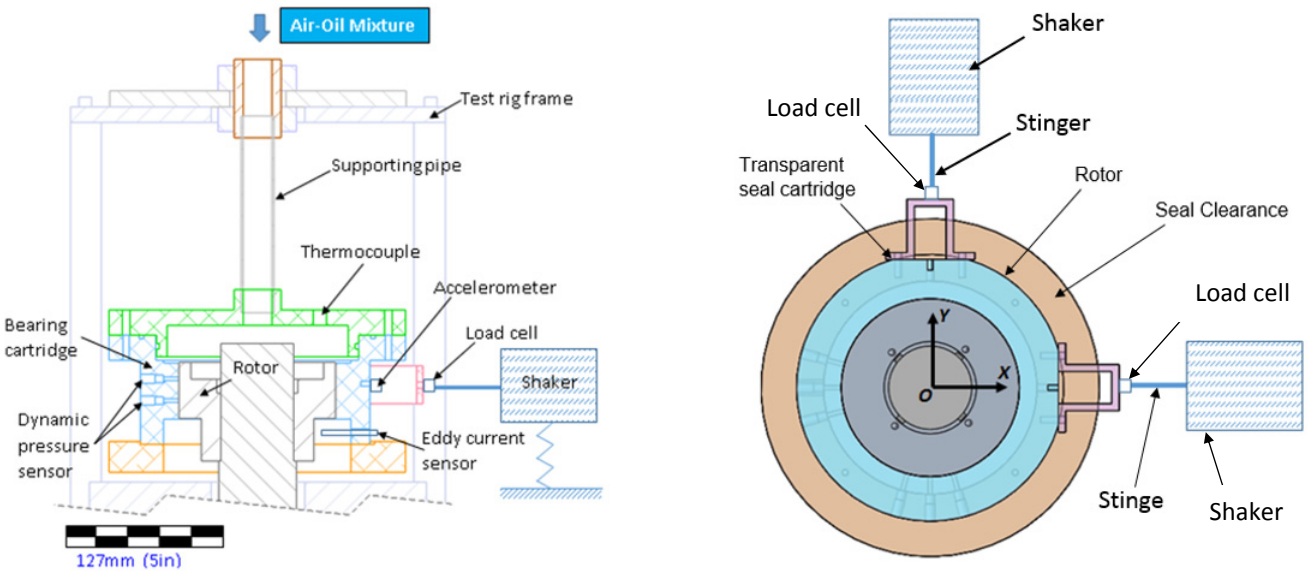

Figure 1. Schematic views of *wet seal* test rig [12].

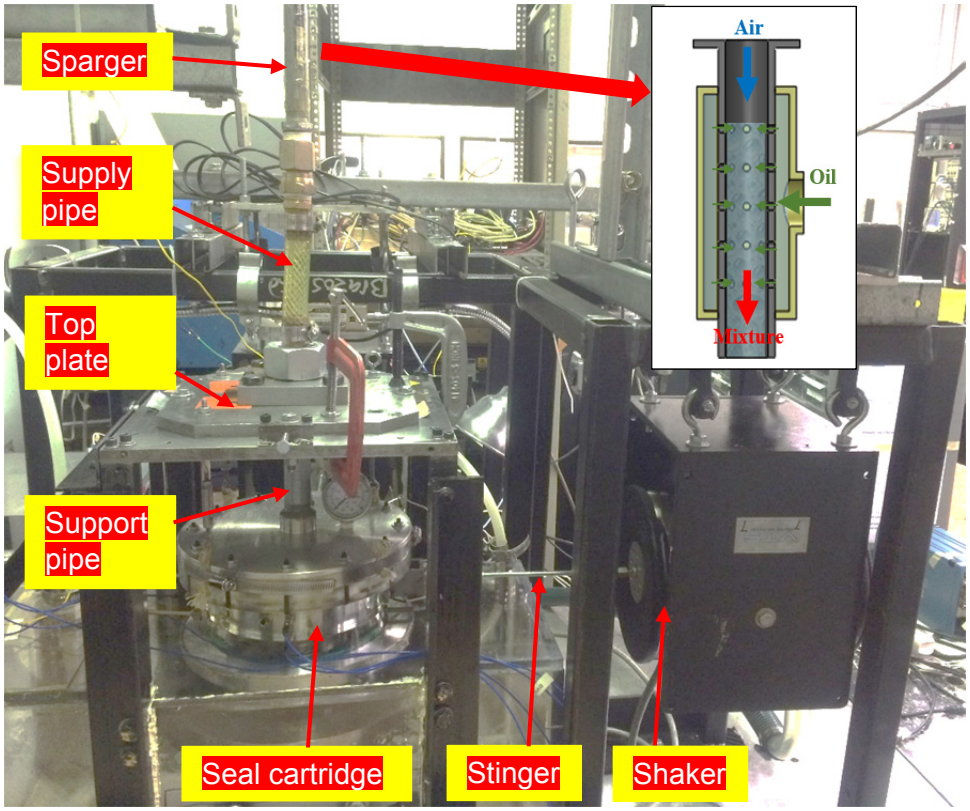

Figure 2. Photograph of *wet seal* test rig. Components labeled.

Table 1. Annular *wet seal* dimensions and fluids parameters .
$\rho_l/\rho_{ga} = 691$, $\mu_l/\mu_{ga} = 900$

Seal Diameter	D	127 mm
Length	L	46 mm
Radial Clearance	c	0.127±0.005mm
Lubricant Parameters		
ISO VG10 Absolute Viscosity	μ_l	18 cP (20ºC)
Density	ρ_l	830 kg/ m^3
Air Viscosity	μ_{ga}	0.02 cP (20ºC)
Density	ρ_{ga}	1.2 kg/m^3 at P_a=1 bar(abs)

In a two-phase flow with oil and gas, the fluid viscosity and density vary with the gas volume fraction (GVF) α_m. For a homogeneous flow [13]:

$$\alpha_m = \frac{1}{1+\left(\frac{1-x}{x}\right)\left(\frac{\rho_g}{\rho_l}\right)} \tag{1}$$

where x is the mixture gas mass fraction, $x = \frac{m_g}{m_g + m_l}$.ρ_g and ρ_l are the gas and liquid density, respectively. In a two-phase flow dominated by gas, a liquid volume fraction (LVF) β is more convenient to describe the flow. The mixture LVF is

$$\beta = \frac{Q_l}{Q_g + Q_l} = 1 - \alpha_m \tag{2}$$

and varies along the seal length as the gas expands. For a homogeneous flow, the mixture density is [13]:

$$\rho_m = \left(\frac{x}{\rho_g} + \frac{1-x}{\rho_l}\right)^{-1} \tag{3}$$

In a homogeneous two-phase flow, the flow density ρ and viscosity μ must satisfy the following conditions:

$$\left.\begin{array}{l} for\ x=0, \rho_m \to \rho_l \\ for\ x=1, \rho_m \to \rho_g \end{array}\right\} ; \left.\begin{array}{l} for\ x=0, \mu_m \to \mu_l \\ for\ x=1, \mu_m \to \mu_g \end{array}\right\} \tag{4}$$

where $x = 0$ represents pure liquid flow, and $x = 1$ represents pure gas flow.

The evaluation of the mixture viscosity (μ_m) is not straightforward, as is a function of the material viscosity of the liquid (μ_l) and gas (μ_g), and either the gas mass fraction (x) or the gas volume fraction (α_m) The archival literature reports many correlations, most applicable to particular flow conditions. **Appendix A** lists 24 viscosity equations. Table 2 lists six common formulas for evaluation of μ_m and to be used for the prediction of flow rate and pressure gradient in two-phase flow along pipes and through small gaps. Recall that the flow in a seal is akin to that trough a small diameter or micro-channel. Awad *et al*. [14, 15] note formulas #19 to #22, obtained from an analogy with the thermal conductivity of porous media, display good agreement with prevailing models such as those from McAdams *et al*. (1942), Cicchitti *et al*. (1960), etc. The results in Ref. [14] show viscosity model #19 is suitable for materials in which the thermal conductivity of the continuous phase is larger than the thermal conductivity of the dispersed phase, like in a foam where the dominant phase is a liquid. Conversely, viscosity model #20 is suitable for a material whose dominant phase is gas. Viscosity model #22 is the arithmetic mean of formulas #19 and #20. The model #20 seems more appropriate for two-phase flow in mini-channels and micro-channels [14]. Note that San Andrés [1] uses viscosity model #17, where μ_m has a distinct raise for flow conditions where the gas mass content (α_m) <0.3, respectively.

Table 2. Formulas for evaluation of effective viscosity in a gas in liquid mixture.

No.	Author	Year	Expression
3	McAdams *et al*.	1942	$\mu_m = \left(\frac{x}{\mu_g} + \frac{1-x}{\mu_l} \right)^{-1}$
9	Cicchitti *et al*.	1960	$\mu_m = x\mu_g + (1-x)\mu_l$
16	Fourar, M., Boris, S.	1995	$\mu_m = (1-\alpha_m)\mu_l + \alpha_m\mu_g + 2\sqrt{\alpha_m(1-\alpha_m)\mu_l\mu_g}$
17	Viscosity used by San Andrés, L.	1998, 2013	$\mu_m = \mu_l \left[1 + 2.5\alpha_m \left(\frac{\mu_g/\mu_l + 0.4}{\mu_g/\mu_l + 1} \right) \right]$, when $\alpha_m \le 0.3$ $\mu_m = (x_+ - 1)\left[\left(\frac{x_+}{\mu_g} - \frac{1}{\mu_+} \right) + \left(\frac{1}{\mu_+} - \frac{1}{\mu_g} \right) x \right]^{-1}$, when $\alpha_m > 0.3$
19	Awad and Muzychka	2008	$\mu_m = \mu_l \frac{2\mu_l + \mu_g - 2(\mu_l - \mu_g)x}{2\mu_l + \mu_g + (\mu_l - \mu_g)x}$
20	Awad and Muzychka	2008	$\mu_m = \mu_g \frac{\mu_l + 2\mu_g + 2(\mu_l - \mu_g)(1-x)}{\mu_l + 2\mu_g - (\mu_l - \mu_g)(1-x)}$

#17, μ_+ and x_+ are the mixture viscosity and mass fraction at α_m =0.3, respectively.

FLOW RATE THROUGH SEAL

The pressure drop of a liquid flowing through a (centered) annular seal is $\Delta P = \Delta P_o + \Delta P_L$, with ΔP_o as the inertial pressure drop at the seal inlet due to the Lomakin effect[1] [16], and ΔP_L is the viscous pressure drop along the seal film land. The Lomakin effect is minor ($\Delta P_o \approx 0$) for a liquid seal operating in the laminar flow regime; hence $\Delta P \approx \Delta P_L = P_s - P_a$. An elementary fluid mechanics analysis shows the liquid mass flow rate is

$$m_l = \rho_l \left(\frac{c^3}{12\mu_l} \frac{\Delta P}{L} \right) \pi D = \rho_l Q_l \qquad (5)$$

Figure 3 shows the measured and predicted mass flow rate (m_l) for an ISO VG10 oil flowing through the seal. The journal is stationary (nonrotating). The measurements and predictions are in agreement and demonstrate the flow rate is proportional to the pressure drop.

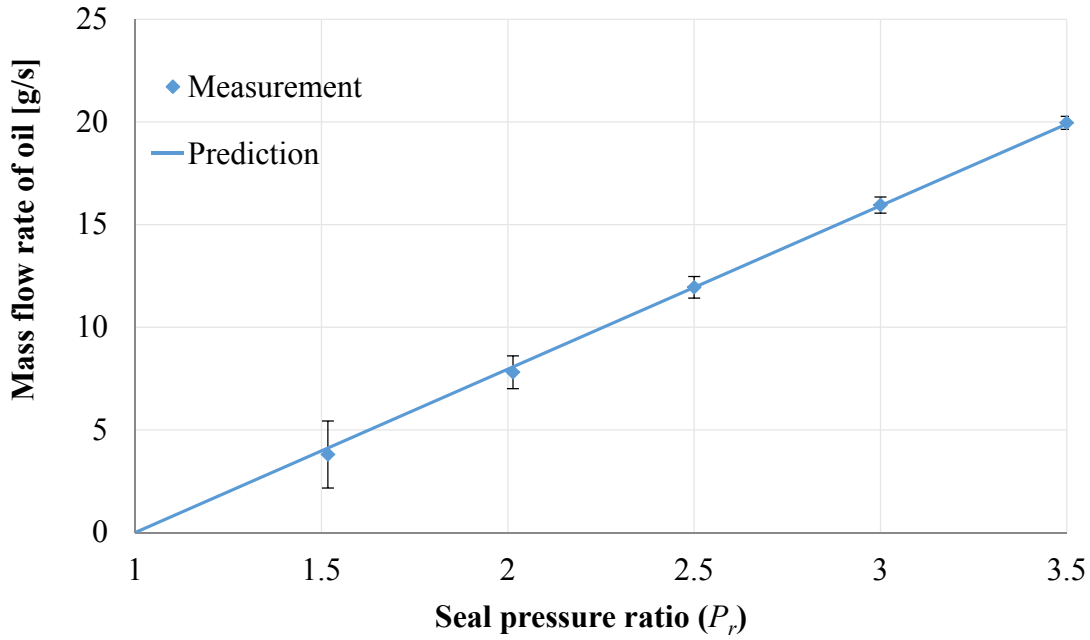

Figure 3. Mass flow rate (m_l) for pure liquid flowing through seal vs. supply/discharge pressure ratio (P_s/P_a). Measurement and prediction. ISO VG 10 oil. Inlet temperature 21°C ~23°C. Stationary (non-rotating) journal.

For a seal operating with a mixture, the GVF (α_m) increases as the mixture flows across the seal due to the drop in pressure which produces the expansion of the gas. Hence, the LVF $\beta = 1-\alpha_m$ decreases. Consequently, ρ_m and μ_m vary along the seal length. HSEALMIX® [1] is a predictive model that delivers the seal flow rate, power loss, and rotordynamic force coefficients for seals operating with a homogeneous two-phase flow.

[1] At the seal inlet plane the fluid pressure (P) undergoes a sudden drop as the fluid accelerates.

For a seal operating with a liquid in gas two-phase flow, the LVF at the seal inlet is

$$\beta_{inlet} = \frac{Q_l}{Q_l + Q_g \frac{P_a}{P_s}} \tag{6}$$

Figure 4 shows the experimental mass flow for a mixture with increasing LVF at the seal inlet and with supply pressure (P_s) equal to 3.0 and 3.5 bar (abs). The figure includes predictions from HSEALMIX®. The experiments and predictions show the seal leakage increases rapidly as the LVF begins to grow ($\beta_{inlet} < 0.1$) since the oil density is much larger than that of the air. For $P_s = 3$ bar (abs), ρ_l/ρ_{ga} =830/3.6 = 231 at the inlet plane. As the LVF increases further ($0.2 < \beta_{inlet} \leq 1$), the rate of leakage increase reduces. Figure 5 supports the findings, the liquid mass fraction (λ) increases rapidly for $\beta_{inlet} < 0.2$, and more moderately for $0.2 < \beta_{inlet} \leq 1$. Note that the predictions shown in Figure 4 employ Fourar and Boris [17] mixture viscosity formula for a homogeneous two-phase flow:

$$\mu_m = \beta_{inlet}\mu_l + (1-\beta_{inlet})\mu_g + 2\sqrt{\beta_{inlet}(1-\beta_{inlet})\mu_l\mu_g} \tag{7}$$

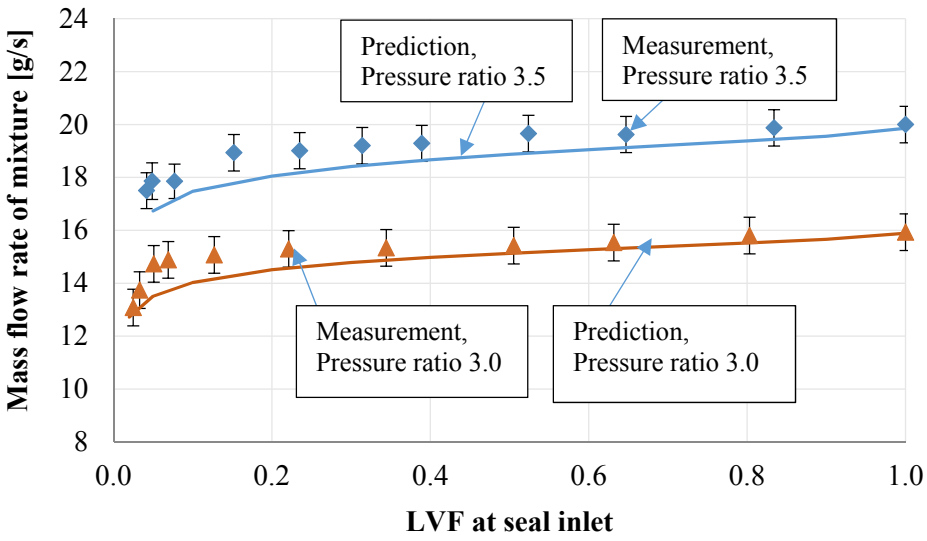

Figure 4. Experimental mixture mass flow rate (m_m) vs. LVF at the seal inlet. Test with inlet temperature 20°C ~22°C. Stationary (non-rotating) journal. Predictions from HSEALMIX® [1].

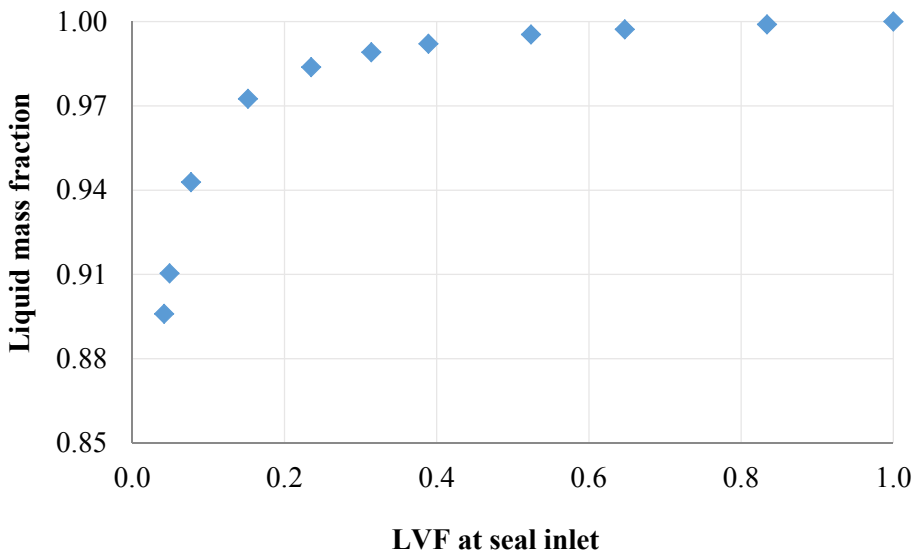

Figure 5. Liquid mass fraction (λ) in mixture vs. LVF at the seal inlet. Test with inlet temperature 20°C ~22°C. Stationary (non-rotating) journal.

The axial flow Reynolds number (Re), the ratio of inertial forces to viscous forces, is

$$\mathrm{Re} = \frac{\rho_m V_z c}{\mu_m} = \frac{m_m}{\pi D \mu_m} \tag{8}$$

Figure 6 shows the predicted axial flow Reynolds number at the seal inlet and exit planes versus the liquid volume fraction (LVF) at the inlet plane. The rapid decrease in Reynolds number is due to the (dramatic) increase in mixture viscosity (μ_m) more than the increase in mass flow (m_m), see Fig. 4. Recall the ratio of fluid viscosities, μ_l/μ_g = 18 cP/0.02 cP ~ 900! The difference in Reynolds number at the inlet and exit planes also relates to the difference in viscosities. Note that Re < 1,000, hence the mixture flows likely under a laminar flow condition. However, the Reynolds number grows to 2,273 when the seal operates with a pure gas; β_{inlet}=0, likely a turbulent flow condition. The results evidence that a small percent of liquid content turns laminar an otherwise turbulent flow. The assertion is valid for a homogenous two-phase flow though.

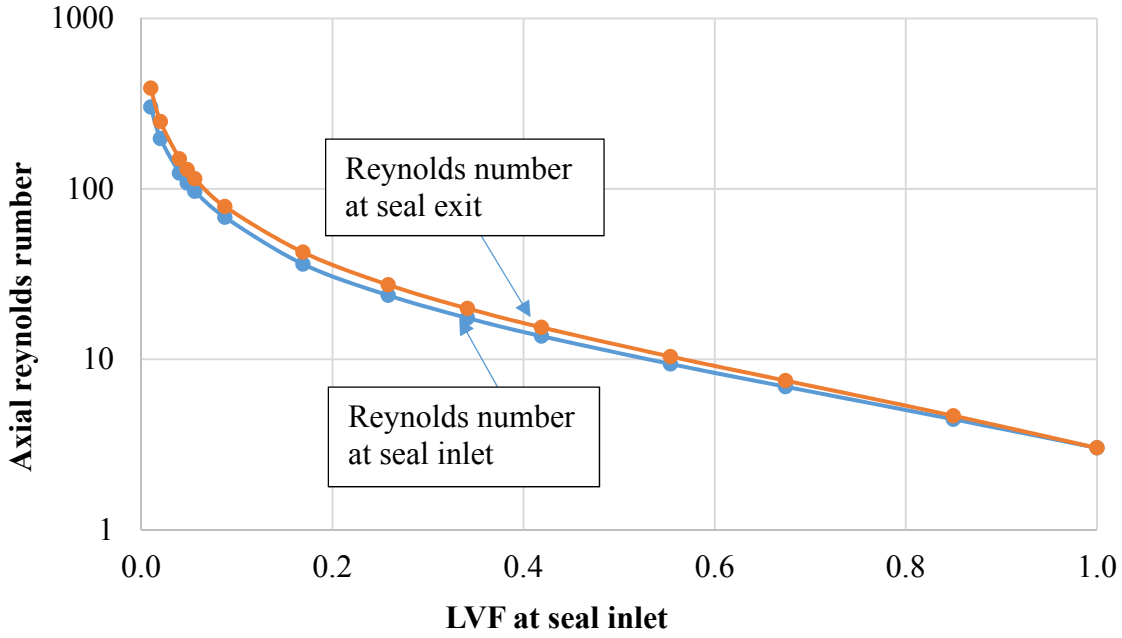

Figure 6. Predicted axial flow Reynolds number at the inlet and exit planes vs LVF at the seal inlet. Test with P_s/P_a = 3.5, inlet temperature 20°C ~22°C. Stationary (non-rotating) journal.

PERIODIC FORCED RESPONSE OF TEST SEAL AND ESTIMATION OF FORCE COEFFICIENTS

The effective mass of the seal cartridge includes the attached instrumentation and a fraction of the mass for the support pipe. The supporting pipe, clamped onto the top plate of the test rig frame in a manner similar to that of a cantilever beam, has an effective mass of approximately 1/4 of its physical mass. Table 3 shows the mass of each component and the estimated effective mass.

Table 3. Measured weight and estimated effective mass of the test seal system

Components	Mass
Seal cartridge	12.60 lb (5.75 kg)
Pipe (1/4 mass)	0.40 lb (0.18 kg)
Sensors	1.70 lb (0.77 kg)
Effective mass M_{SC}	14.7 lb (6.7 kg ± 0.04 kg)

In static load tests (no oil/ no gas is supplied to the seal), a force gauge pushes and pulls the seal cartridge along the X and Y directions, two eddy current sensors measure the displacements exerted by static load along the two directions, i.e., $F_{XS} \rightarrow X_{XS}$, with F_{XS} as a static load and X_{XS} is the ensuing displacement. Similarly, F_{SY}

→ $Y_{SY.}$ The test rig structural static stiffness (K_S) = dF_S/X_S. Figure 7 shows the seal cartridge displaces linearly for applied force F_S = -55 N to +55N. The structural stiffness coefficients are K_{SX}=708±28 kN/m and K_{SY}=736±28 kN/m (~4% difference).

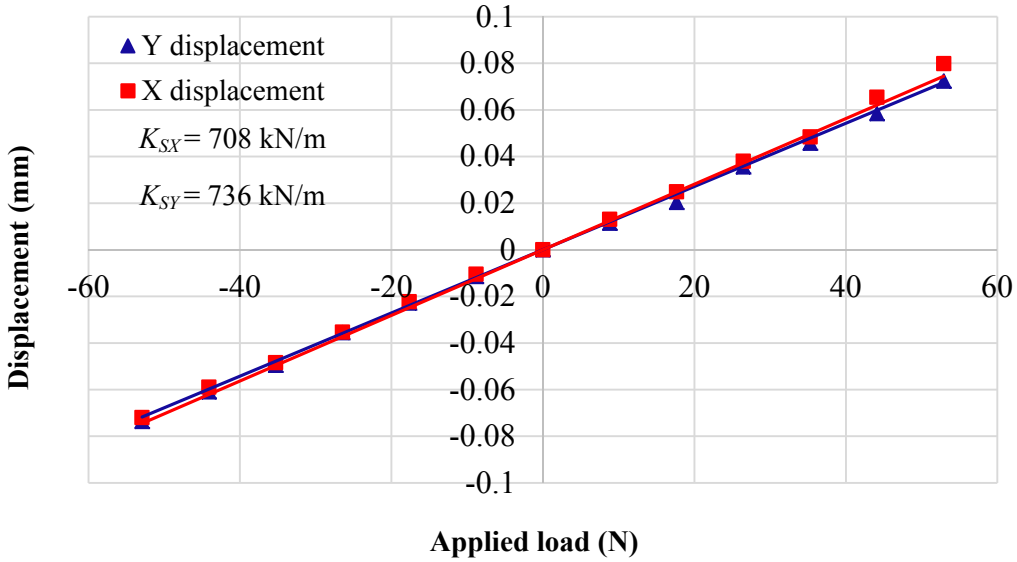

Figure 7. Seal cartridge static displacement vs. applied static load. Dry test system.

Unidirectional Periodic Load Tests on *Dry* Structure

To identify the structure stiffness K_S and damping C_S, the rotor is stationary (non-rotating) and the seal clearance is "dry" (with only air at ambient condition). The shakers, via long stingers, excite the seal cartridge with a unidirectional load with excitation frequency ranging from 30 Hz to 200 Hz, in steps of 10 Hz. The data acquisition system records 12,800 samples over a time span of 0.64s. The parameter identification procedure follows that described by San Andrés [19].

Table 4 shows the estimated system direct force coefficients of the dry system. M_{SC} is the seal cartridge mass, and C_S and K_S are the structure damping and stiffness coefficients, respectively. Cross-coupled coefficients are negligible.

Table 4. Test system (dry) structure force coefficients.

Stiffness K_{SXX}, K_{SYY}	690 ±7, 690 ±7 kN/m
Damping C_{SXX}, C_{SYY}	213 ±11, 108 ±11 N.s/m
Mass M_{SCXX}, M_{SCYY}	7.0 ±0.5, 6.8 ±0.5 kg
Natural frequency* f_{nx}, f_{ny}	50, 51 Hz
Damping ratio** ξ_X, ξ_Y	0.05, 0.03

*: $f_n = \sqrt{K_s/M_{SC}}$, ** $\xi = C/(2\sqrt{K_s M_{SC}})$

Note that from static load tests the structure stiffnesses are K_{SX}=708±28 kN/m and K_{SY}=736±28 kN/m, and the estimated effective mass M_{SC}= 6.7 kg. The force coefficients obtained from the periodic load tests, see Table 4, are within the uncertainty range of the static parameters, except $K_{SY.}$ This could be due to misalignment from the applied load, for example. The 4% difference is deemed acceptable. Note the identification process delivers negligible cross-coupled force coefficients.

Force Coefficients for Seal Operating With Liquid in Gas Mixture

The test procedure is to first open the valve of the air supply line; and next, the oil supply pump is turned on to deliver oil (ISO VG 10) into the sparger element for mixing with the air. Figure 9 (a) shows that the annular seal operates with a liquid in a gas mixture. The mixture flows into the seal to later discharge into a plenum. The mixture, the "yellow" fluid in Figure 8 (a) stays in the container for about three minutes, until most of the air bubbles released into the atmosphere. A return pump then brings the remaining oil to the oil reservoir for recirculation[2].

When the mixture enters the plenum shown in Figure 8 (b) the pressure difference $(P_s\text{-}P_a)$ applies an upward force to the seal cartridge, $F_u = (P_s\text{-}P_a)A_s$, where $A_s = ¼\ \pi\ D_T^2$ (D_T = 0.147m, A_S = 0.017 m^2) is the area of pressure action. Unfortunately, this upwards creates a bending moment on the support pipe and the seal cartridge tilts and displaces to an off-centered position. To offset this (undesirable) displacement, as shown in Figure 8 (a), four elastic strings, connecting the cartridge to the top plate of the test rig, are tightened to bring the seal to its original position after being pressurized. Because the upward force varies with a change in seal supply pressure P_s, the procedure requires to adjust the strings each time the seal supply pressure (P_s) changes. Most importantly, by tightening the strings, the lateral stiffness (K_S) of the structure changes, i.e., with a supply pressure of 3.0 bar (abs) and with a taut string, the structure stiffness increases form K_{SXX} =690 kN/m to K_{SXX} = 794 kN/m, and K_{SYY} = 690 kN/m, and K_{SYY} = 821kN/m. That is, the stiffness increases by 15% and 18%, respectively. The variation also increases the *dry* system natural frequency by up to 9%.

Note that for the tests with a supply pressure P_s= 2.0 bar (abs), the seal cartridge displaces ~1/4 mil (6 μm) away from its centered position. The seal eccentricity is small (<< c), and hence the strings were not tightened to bring the seal cartridge to its center. Consequently, the structure force coefficients are as reported in Table 4.

[2] A coalescer or bubble eliminator will be installed soon to ensure the return lubricant is free of air.

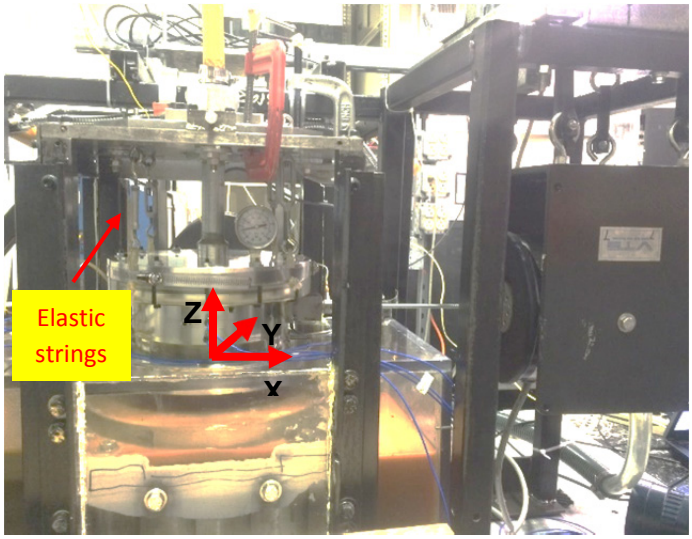

Figure 8(a) Photograph of *mixture* in test rig.

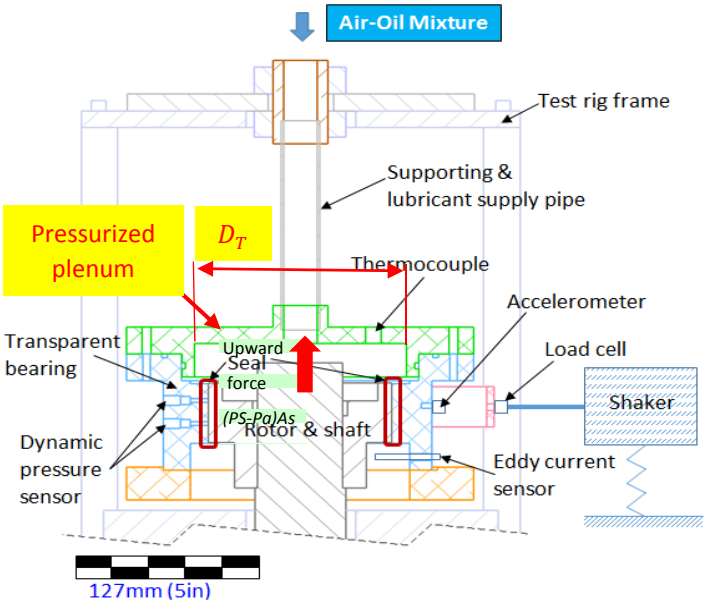

Figure 8(b) Schematic view of upward force applied to cartridge and support pipe.

The parameter identification process follows Ref. [18] as it models the test system as a two-degree of freedom mechanical system with lateral displacements X and Y. Figure 9 [19] depicts an idealized view of the test system as a mechanical structure with stiffness (K) and viscous damping (C) coefficients. The structure and seal act in parallel as they *see* the same lateral displacements. For small amplitude motions about an equilibrium position, the linearized system equations of motion for the test system is:

$$\mathbf{M}\,\ddot{\mathbf{z}} + \mathbf{C}\,\dot{\mathbf{z}} + \mathbf{K}\,\mathbf{z}_{(t)} = \mathbf{F}_{(t)} \qquad (9)$$

where $\mathbf{F} = [F_X, F_Y]^T$ is the vector of applied external force, and $\mathbf{z}=[X_{(t)}, Y_{(t)}]^T$ and $\boldsymbol{a}= [a_X, a_Y]^T$ are the ensuing seal cartridge displacement and acceleration vectors, respectively. Above, $\mathbf{K}=[\,K_{XX}\,K_{XY}\,|\,K_{YX}\,K_{YY}\,]$ and $\mathbf{C}=[\,C_{XX}\,C_{XY}\,|\,C_{YX}\,C_{YY}\,]$ are the test system matrices of stiffness and viscous damping coefficients. Also $\mathbf{M}=[\,M_{XX}\,M_{XY}\,|\,M_{YX}\,M_{YY}]$. Note

$$\mathbf{M}=\mathbf{M_{SC}}+\mathbf{M_{seal}},\ \mathbf{K}=\mathbf{K_S}+\mathbf{K_{seal}},\ \mathbf{C}=\mathbf{C_S}+\mathbf{C_{seal}} \qquad (10)$$

Above $\mathbf{M_{SC}} = [\,M_{SCXX}\,0\,|\,0\,M_{SCYY}\,]$ represents the seal cartridge effective mass, and $\mathbf{K_S}$, $\mathbf{C_S}$ denote the structure stiffness and (remnant) damping. The seal force coefficients are denoted by the matrices $(\mathbf{K, C, M})_{\mathbf{seal}}$.

[3]In forced response tests, single frequency unidirectional loads are exerted on the seal cartridge along the X and Y directions, i.e., $\mathbf{F_X}=[f_X=f_o\,\varepsilon^{\iota\omega t}\,,\,0]^T$ and $\mathbf{F_Y}=[0,\,f_Y=f_o\,e^{\iota\omega t}]^T$ where ω is an excitation frequency and f_o is a

[3] From here on the report reproduces ad-verbatim material in Ref. [12]

load amplitude. ι is the imaginary unit. The ensuing cartridge accelerations $\mathbf{a_X}=[a_{XX},\ a_{YX}]^T$ and displacements $\mathbf{z_X}=[X_X,\ Y_X]^T$ are recorded. Similarly, $\mathbf{F_Y} \rightarrow \mathbf{a_Y}=[a_{XY},\ a_{YY}]^T$ and $\mathbf{z_Y}=[X_Y,\ Y_Y]^T$. In the frequency domain, the equation of the motion for the test system is

$$[\mathbf{K} - \omega^2 \mathbf{M} + \iota\, \omega\ \mathbf{C}\ ]\ [\mathbf{Z_X}\ |\ \mathbf{Z_Y}]\ e^{i\omega t} = = [\ f_o,0\ |\ 0,f_o\ ]\ e^{i\omega t} \qquad (11)$$

Above $\mathbf{Z}_{(\omega)}\ e^{i\omega t} = \mathrm{DFT}[\mathbf{z}_{(t)}]$ is the fundamental Fourier series component of a displacement vector. The system complex stiffness $\mathbf{H}=[\mathbf{K}- \omega^2 \mathbf{M} + \iota\, \omega\, \mathbf{C}\ ]$ is determined from solution of

$$\mathbf{H}_{(\omega)} = [\ f_o,0\ |\ 0,f_o\ ]\ [\mathbf{Z_X}\ |\ \mathbf{Z_Y}]^{-1} \qquad (12)$$

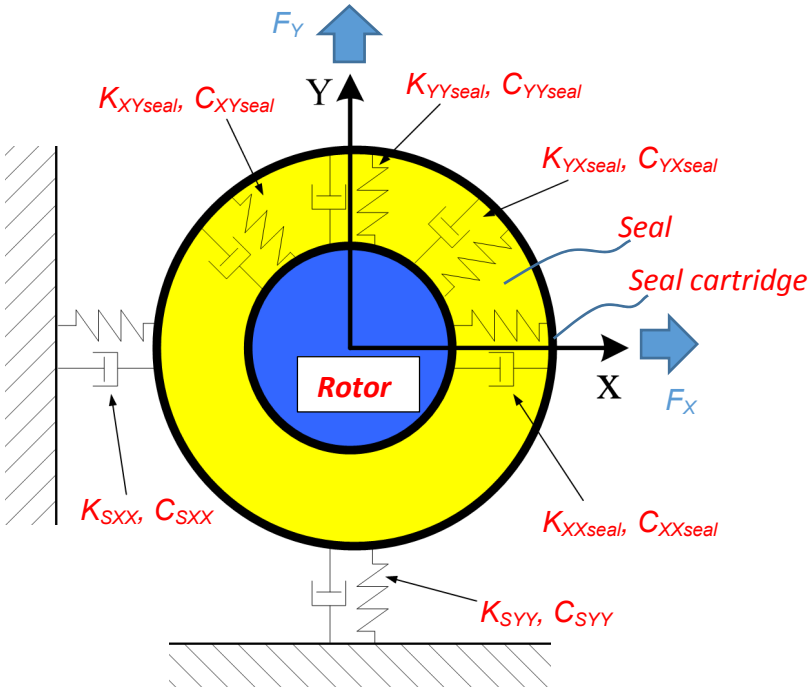

Figure 9. Schematic view of idealized two degree of freedom structure-seal system for parameter coefficient identification [19].

With a stationary rotor (non-rotating) and a supply pressure of P_s=2 bar(abs), the seal is supplied with an oil in gas mixture with a liquid volume fraction β_{inlet}=0% (pure air), 2% and 4%. The corresponding liquid mass fraction content (λ equals0%, 90% and 95%, respectively). Dynamic load tests are conducted with an excitation frequency ranging from 30 Hz to 200 Hz, in steps of 10 Hz. The complex stiffness $\mathbf{H}_{(\omega)}$ is determined from the measured loads and displacements by solving Eq. (12).

Figure 10 displays the real and imaginary parts of the complex stiffnesses H_{XX} and H_{YY}. Note that cross-coupled stiffnesses H_{XY} and H_{YX} are negligible compared to the direct terms and are shown in Appendix C. In addition, note the difference in vertical scale for Im(H), in particular for the all air condition (λ =0 → β_{inlet} = 0),

the seal shows very little damping. The real part of the complex stiffness coefficient, Re(H) can be accurately characterized by a stiffness (K) and added mass terms (M), i.e., Re(H) ← (K-$M\omega^2$), over the range of excitation frequency, 30-200 Hz., as shown in Figure 10(b), left graph, for an inlet LVF at 2%.

Table 5 lists the identified direct stiffness (K_{XX} ,K_{YY})$_{seal}$ and mass coefficients (M_{XX} ,M_{YY})$_{seal}$. The virtual masses increase with liquid volume content to become a sizable magnitude, comparable to the cartridge mass (M_{SC}=~6.9 kg). The seal stiffness is also larger than the structure stiffness (K_S~0.69 MN/m). In Figure 4, the natural frequency of test system is approximately 80Hz (> ω_n=50Hz for the "dry" system), thus denoting the pressure drop across the seal, either a mixture or pure gas, raises the system direct stiffnesses, K_{XX} and K_{YY}.

Note that in Figure 10, the natural frequency of the test system remains at ~ 80 Hz as the inlet LVF increases to 4%. This implies the system stiffness and mass coefficients increase in the same proportion, likely due to the raise of the effective density in the mixture.

Table 5. Direct stiffness and mass coefficients for *wet* seal supplied with oil in gas mixture. Tests with supply pressure P_S=2.0 bar (abs), ambient pressure P_a=1 bar (abs), inlet temperature 20°C. Stationary (non-rotating) journal [12].

Structure force coefficients (Table 4) K_{SXX}= K_{SYY}=0.69 MN/m, M_{SCXX}=7.0 kg, M_{SCYY}=6.8 kg.

LVF at seal inlet	Liquid mass fraction	K_{XXseal} MN/m	K_{YYseal} MN/m	M_{XXseal} kg	M_{YYseal} kg
0	0	1.4	1.0	0	0
2%	90%	1.5	1.3	0.3	0.7
4%	95%	2.5	1.3	1.2	0.9

In Figure 10, Im(H) is not proportional to the excitation frequency, thus cannot be characterized by a constant damping (C), Im(H) ← $C\omega$. That is, a viscous damping model is not adequate for a *wet* seal. For operation with all gas and two oil in gas mixture conditions, Figure 11 depicts $C_{seal(\omega)}$=(Im(H)/ω-C_s) versus excitation frequency. The coefficients are shown in logarithmic scale to make evident their variation. Note the large effect of a small content of liquid (β_{inlet}=2% and 4%) that produces an increase of nearly 10 and 20 times the damping coefficient of the seal when supplied with air only (LVF=0%). That is, a very small amount of liquid makes the *wet* seal generate significant dissipative forces. Incidentally, note Im(H) > Re(H), as the excitation frequency grows.

The typical maximum uncertainties for the estimated stiffness, damping and mass coefficients are ~ ½ %, 2% and 6% of the quoted physical magnitude for each coefficient, respectively. Note that each dynamic forced response test was conducted no less than five times, each case showing repeatable results.

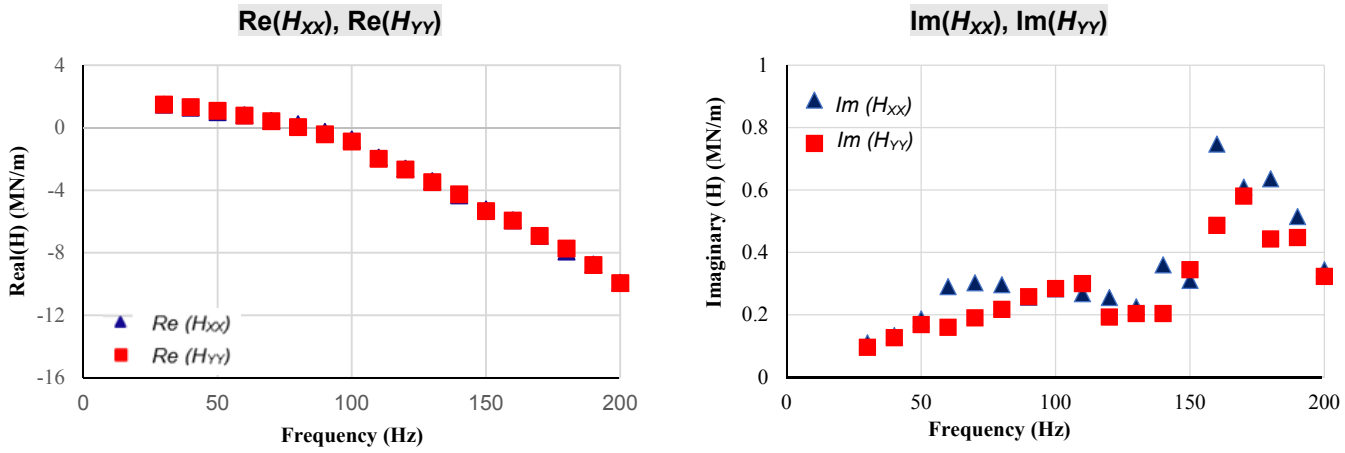

(a) β_{inlet} = 0, all gas (m_m=6.0±0.8 g/s)

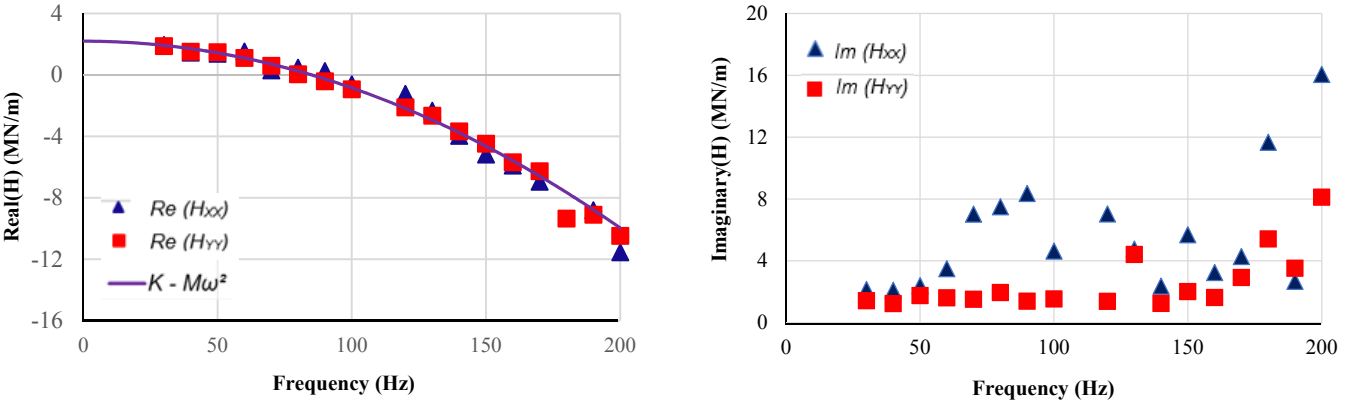

(b) β_{inlet} = 0.02, λ=0.90 (m_m=6.0±0.2 g/s)

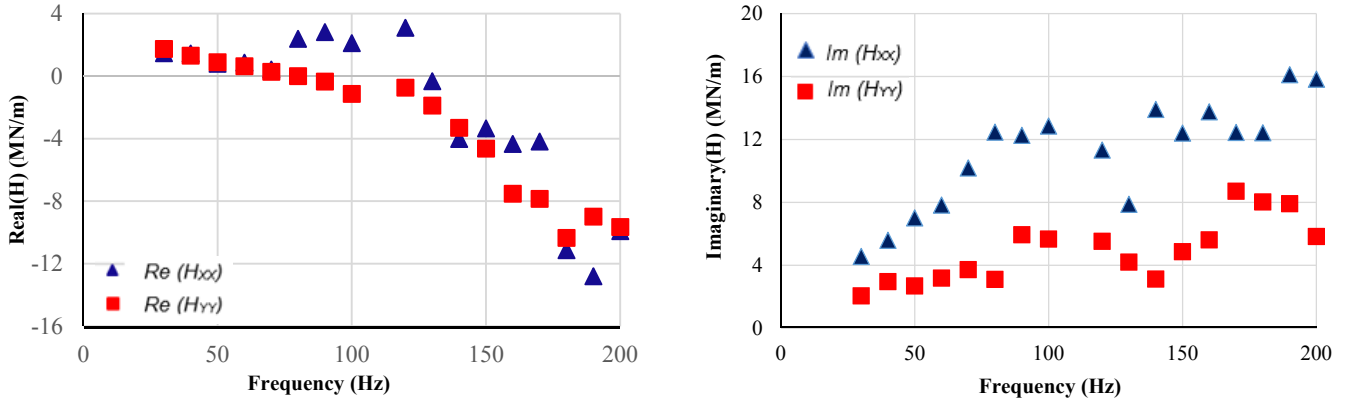

(c) β_{inlet} = 0.04, λ= 0.95 (m_m=7.0±0.2 g/s)

Figure 10. Real and imaginary parts of complex stiffnesses (H_{XX}, H_{YY}) for *wet seal* supplied with an oil in air mixture with a liquid volume fraction at the inlet plane (β_{inlet}) equal to (a) 0% (all gas), (b) 2%, and

(c) 4%. Stationary (non-rotating) journal. Tests with supply pressure P_S=2.0 bar(abs), ambient pressure P_a=1 bar(abs), inlet temperature 20°C [12].

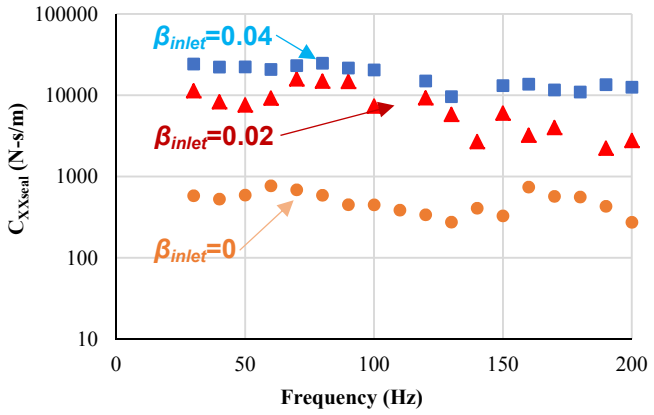

(a) C_{XXseal}

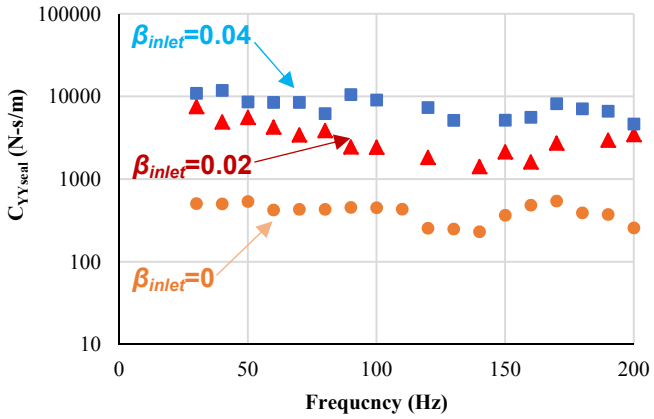

(a) C_{YYseal}

Figure 11. Direct damping coefficients (C_{XX}, C_{YY})$_{seal}$ versus excitation frequency for *wet seal* supplied with oil in gas mixture with a liquid volume fraction at the inlet plane (β_{inlet}) equal to 0% (all gas), 2%, and 4%. Stationary (non-rotating) journal. Tests with supply pressure P_S=2.0 bar(abs), ambient pressure P_a=1 bar(abs), inlet temperature 20°C [12].

CONCLUSION

This report shows measurements of mass flow rate and dynamic force coefficients for an annular seal (L/D=0.36) supplied with a homogeneous mixture of ISO VG 10 oil and air and delivered at ambient temperature. The mixture flows through the seal clearance (0.127 mm) and exits to ambient pressure. The large difference in density between the liquid (oil) and gas (air) determines that the liquid mass content (λ) in the mixture be rather large even when the liquid volume fraction (β) is just at a low percentage.

In tests conducted with a stationary (non-rotating) journal and with a supply pressure P_S=3.5 bar(abs), the mass flow rate increases rapidly as the inlet LVF increases from 0.04 to 0.2. Since the liquid mass fraction λ~1 for β_{inlet}>0.30, the growth in mass flow reduces as the LVF raises towards an all liquid condition (β=1).

In dynamic force (single frequency) response measurements conducted with a supply pressure of P_S=2 bar(abs) and a non-rotating journal, the test system direct dynamic stiffness, Re(H), is well characterized by a static stiffness (K) and added mass (M) coefficients, i.e., (K-$M\,\omega^2$)→ Re(H), for operation with either a pure gas or mixtures with β_{inlet} = 2% and 4%. On the other hand, the quadrature of the complex stiffness, Im(H), is not proportional to frequency for the *wet* seal. Damping coefficients attained for operating conditions with a small volume fraction of oil in gas (4%) can be (approximately) twenty times larger than those obtained for the pure gas condition. The effect of a few *droplets* of liquid on affecting the test system forced response is overwhelming.

Presently, the tests conducted without journal rotation and with a low supply/discharge pressure (max. 3.5) determine the mixture flows regularly through the seal; that is, the flow regime is laminar. Future work will operate the test facility with journal rotation (6 krpm [40 m/s]) and at a higher supply pressure while delivering a mixture of increasing liquid content. In addition, the measurements of *wet* seal flow rate and force coefficients will serve to benchmark predictions derived from Ref. [1].

REFERENCES

[1] San Andrés, L. S., 2012, "Rotordynamic Force Coefficients of Bubbly Mixture Annular Pressure Seals," ASME J. Eng. Gas Turbines Power, **134**(2), p. 022503.

[2] Vannini, G., Bertoneri, M., Del Vescovo, G. and Wilcox, M., 2014, "Centrifugal Compressor Rotordynamics in Wet Gas Conditions," Proceedings of the 43rd Turbomachinery & 30th Pump Users Symposia, Houston, TX, September 23-25.

[3] Bertoneri, M., Wilcox, M., Toni, L. and Beck, G., 2014, "Development of Test Stand for Measuring Aerodynamic, Erosion, and Rotordynamic Performance of a Centrifugal Compressor Under Wet Gas Conditions," ASME Paper GT2014-25349, Proceedings of ASME Turbo Expo 2014: Turbine Technical Conference and Exposition, Dösseldorf, Germany, June 16-20.

[4] Brennen, L., Bjorge, T., Gilarranz, J., 2005, "Performance Evaluation of a Centrifugal Compressor Operating Under Wet Gas Conditions," 34th Turbomachinery Symposium, Houston, TX, December 12-15.

[5] Beatty, P. A., and Hughes, W. F., 1987, "Turbulent Two-Phase Flow in Annular Seals," ASLE Trans., **30**(1) pp. 11-18.

[6] Beatty, P. A., and Hughes, W. F., 1990, "Stratified Two-Phase Flow in Annular Seals," ASME J. Tribol., **112**(2) pp. 372-381.

[7] Iwatsubo, T., and Nishino, T., 1993, "An Experimental Study on the Static and Dynamic Characteristics of Pump Annular Seals," 7th Workshop on Rotordynamic Instability Problems in High Performance Turbomachinery.

[8] Arauz, G. L., and San Andrés, L., 1997, "Analysis of Two-Phase Flow in Cryogenic Damper Seals - Part I: Theoretical Model," ASME J. Tribol., **120**, pp. 221-227.

[9] Arauz, G. L., and San Andrés, L., 1997, "Analysis of Two-Phase Flow in Cryogenic Damper Seals - Part II: Model Validation and Predictions," ASME J. Tribol., **120**, pp. 228-233.

[10] Oike, M., Nosaka, M., Kikuchi, M., 1999, "Two-Phase Flow in Floating-Ring Seals for Cryogenic Turbopumps," Tribol. Trans., **42**(2) pp. 273-281.

[11] Arghir, *et al*., 2009, "Rotordynamic analysis of textured annular seals with mutiphase (bubbly) flow," Workshop: "Dynamic Sealing under Severe Working Conditions" EDF-LMS Futuroscope, October 5.

[12] San Andrés, L., Liu Q and Lu X., 2015, "Measurements of Leakage and Force Coefficients in a Short Length Annular Seal Operating With a Gas in Oil Mixture," STLE Annual Meeting Extended Abstract, Dallas, US, May 17-21.

[13] Thome, J.R., 2004, "Engineering Data Book III," Wolverine Tube, Inc., Huntsvile, AL, USA, http://www.wlv.com/products/ databook/db3/DataBookIII.pdf.

[14] Awad, M.M., Muzychka, Y.S., 2008, "Effective Property Models of Homogeneous Two-Phase Flows," Exp. Therm. Fluid SCI, doi:10.1016/j.expthermflusci.2008.07.006.

[15] Awad, M. M., 2012, "Two-Phase Flow, Chapter 11," http://dx.doi.org/10/5772/76201.

[16] San Andrés, L., 2014, "Annular Pressure Seals," Lubrication Notes 12 (a), Texas A&M University Digital Libraries, https://repository.tamu.edu/handle/1969.1/93252.

[17] Fourar, M., Bories, S., 1995, "Experimental Study of Air-Water Two-Phase Flow through a Fracture (Narrow Channel)", Int. J. Multiphase Flow, **21**, pp. 621-637.

[18] Childs, D.W., Hale, K., 1994, "A Test Apparatus and Facility to Identify The Rotordynamic Coefficients of High-Speed Hydrostatic Bearings," N94-3419, NASA Technical Report.

[19] San Andrés, L., 2014, "Experimental Identification of Bearing Force Coefficients," Lubrication Notes 14, Texas A&M University Digital Libraries, https://repository.tamu.edu/handle/1969.1/93254.

[20] Mahecha, P., 2011, "Experimental Dynamic Forced Performance of a Centrally Grooved, End Sealed Squeeze Film Damper," M.S. Thesis, Texas A&M Univ., College Station, TX., USA.

Appendix A. Formulas for the Viscosity of a Mixture

Table A. ***1*** lists 24 published formulas to predict the effective viscosity (μ_m) of a two-phase flow. Most formulas are to be used to predict a pressure gradient for flow thorugh pipes. The two-phase flow is regarde as homogeneous, with the gas and liquid phases traveling at a same speed. Below μ_l, μ_g are the viscosity of the liquid and gas, ρ_l, ρ_g and ρ_m represent the density of the liquid, gas, and mixture, respectively. α_m is the gas volume fraction, x is the gas mass fraction, H_l is the liquid holdup. μ_+ and $x_+$are the mixture viscosity and mass fraction at α_m=0.3, respectively.

Table A. 1. Effective viscosity models for a gas-liquid mixture

No.	Author	Year	Expression
1	Arrhenius	1887	$\mu_m = \mu_l^{1-\alpha_m} \mu_g^{\alpha_m}$
2	Bingham	1906	$\mu_m = \frac{1-\alpha_m}{\mu_l} + \frac{\alpha_m}{\mu_g}$
3	McAdams *et al*.	1942	$\mu_m = \left(\frac{x}{\mu_g} + \frac{1-x}{\mu_l} \right)^{-1}$
4	Davidson *et al*.	1943	$\mu_m = \mu_l \left[1 + x \left(\frac{\rho_l}{\rho_g} - 1 \right) \right]$
5	Vermeulen *et al*.	1955	$\mu_m = \frac{\mu_l}{\alpha_m} \left[1 + \left(\frac{1.5\mu_g (1-\alpha_m)}{\mu_l + \mu_g} \right) \right]$
6	Akers *et al*.	1959	$\mu_m = \frac{\mu_l}{(1-x) + x\sqrt{\rho_l / \rho_g}}$
7	Hoogendoorn	1959	$\mu_m = \mu_l^{H_l} \mu_g^{1-H_l}$
8	Bankoff	1960	$\mu_m = H_l \mu_l + (1-H_l) \mu_g$
9	Ciccihitti *et al*.	1960	$\mu_m = x\mu_g + (1-x) \mu_l$
10	Owen	1961	$\mu_m = \mu_l$
11	Dukler *et al*.	1964	$\mu_m = \rho_m \left[x \frac{\mu_g}{\rho_g} + (1-x) \frac{\mu_l}{\rho_l} \right]$

12	Oliemans	1976	$\mu_m = \frac{\mu_l(1-\alpha_m)+\mu_g(1-H_l)}{(1-\alpha_m)+(1-H_l)}$
13	Beattie and Whalley	1982	$\mu_m = \mu_l(1-\alpha_m)(1+2.5\alpha_m)+\mu_g\alpha_m$
15	Lin *et al*.	1991	$\mu_m = \frac{\mu_l\mu_g}{\mu_g + x^{1.4}(\mu_l-\mu_g)}$
16	Fourar and Boris	1995	$\mu_m = (1-\alpha_m)\mu_l + \alpha_m\mu_g + 2\sqrt{\alpha_m(1-\alpha_m)\mu_l\mu_g}$
17	Viscosity model used by San Andrés	2011	$\mu_m = \mu_l\left[1+2.5\,\alpha_m\left(\frac{\mu_g/\mu_l+0.4}{\mu_g/\mu_l+1}\right)\right], when\ \alpha_m \le 0.3$ $\mu_m = (x_+-1)\left[\left(\frac{x_+}{\mu_g}-\frac{1}{\mu_+}\right)+\left(\frac{1}{\mu_+}-\frac{1}{\mu_g}\right)x\right]^{-1}, when\ \alpha_m > 0.3$
18	Garcia *et al*.	2003	$\mu_m = \mu_l\left(\frac{\rho_m}{\rho_l}\right) = \frac{\mu_l\rho_g}{x\rho_l+(1-x)\rho_g}$
19	Awad and Muzychka (1)	2008	$\mu_m = \mu_l\frac{2\mu_l+\mu_g-2(\mu_l-\mu_g)x}{2\mu_l+\mu_g+(\mu_l-\mu_g)x}$
20	Awad and Muzychka (2)	2008	$\mu_m = \mu_g\frac{\mu_l+2\mu_g+2(\mu_l-\mu_g)(1-x)}{\mu_l+2\mu_g-(\mu_l-\mu_g)(1-x)}$
21	Awad and Muzychka (3)	2008	$\mu_m = \frac{1}{2}\left[\mu_l\frac{2\mu_l+\mu_g-2(\mu_l-\mu_g)x}{2\mu_l+\mu_g+(\mu_l-\mu_g)x}+\mu_g\frac{\mu_l+2\mu_g+2(\mu_l-\mu_g)(1-x)}{\mu_l+2\mu_g-(\mu_l-\mu_g)(1-x)}\right]$
22	Awad and Muzychka (4)	2008	$\mu_m = \frac{1}{4}\left[(3x-1)\mu_g+(3(1-x)-1)\mu_l+\sqrt{\left[(3x-1)\mu_g+(3(1-x)-1)\mu_l\right]^2+8\mu_l\mu_g}\right]$
23	Muzychka *et al*. (1)	2011	$\mu_m = \left[\mu_l\frac{2\mu_l+\mu_g-2(\mu_l-\mu_g)x}{2\mu_l+\mu_g+(\mu_l-\mu_g)x} * \mu_g\frac{\mu_l+2\mu_g+2(\mu_l-\mu_g)(1-x)}{\mu_l+2\mu_g-(\mu_l-\mu_g)(1-x)}\right]^{0.5}$
24	Muzychka *et al*. (2)	2011	$\mu_m = \left[2\mu_l\frac{2\mu_l+\mu_g-2(\mu_l-\mu_g)x}{2\mu_l+\mu_g+(\mu_l-\mu_g)x} * \mu_g\frac{\mu_l+2\mu_g+2(\mu_l-\mu_g)(1-x)}{\mu_l+2\mu_g-(\mu_l-\mu_g)(1-x)}\right] /$ $\left[\mu_l\frac{2\mu_l+\mu_g-2(\mu_l-\mu_g)x}{2\mu_l+\mu_g+(\mu_l-\mu_g)x}+\mu_g\frac{\mu_l+2\mu_g+2(\mu_l-\mu_g)(1-x)}{\mu_l+2\mu_g-(\mu_l-\mu_g)(1-x)}\right]$

Appendix B: Uncertainly analysis

Uncertainty of LVF. The liquid volume fraction (LVF) at the seal inlet (β_{inlet}) cannot be directly measured in the tests. The LVF (β_{inlet}) is derived from

$$\beta_{inlet} = \frac{Q_l}{Q_l + Q_g \frac{P_a}{P_s}} = \frac{Q_l P_s}{Q_l P_s + Q_g P_a} \tag{B.1}$$

where Q_g and Q_l are measured flow rates of gas an liquid streams supplied at pressure P_s. The relative uncertainty of the parameter β_{inlet} is

$$\frac{U_{\beta_{inlet}}}{\beta_{inlet}} = \left[\left(\frac{\partial \beta_{inlet}}{\partial Q_l} \frac{U_{Q_l}}{\beta_{inlet}} \right)^2 + \left(\frac{\partial \beta_{inlet}}{\partial Q_g} \frac{U_{Q_g}}{\beta_{inlet}} \right)^2 + \left(\frac{\partial \beta_{inlet}}{\partial P_s} \frac{U_{P_s}}{\beta_{inlet}} \right)^2 \right]^{1/2} \tag{B.2}$$

where the derivatives are

$$\frac{\partial \beta_{inlet}}{\partial Q_l} = \frac{Q_g P_s P_a}{(Q_l P_s + Q_g P_a)^2} \tag{B.3}$$

$$\frac{\partial \beta_{inlet}}{\partial Q_g} = -\frac{Q_l P_s P_a}{(Q_l P_s + Q_g P_a)^2} \tag{B.4}$$

$$\frac{\partial \beta_{inlet}}{\partial P_s} = \frac{Q_g Q_l P_a}{\left(Q_l P_s + Q_g P_a\right)^2} \tag{B.5}$$

And the uncertainty in seal inlet LVF is

$$\frac{U_{\beta_{inlet}}}{\beta_{inlet}} = \frac{1}{Q_l P_s + Q_g P_a} \left[\left(\frac{Q_g P_a}{Q_l} U_{Q_l} \right)^2 + \left(-P_a U_{Q_g} \right)^2 + \left(\frac{Q_g P_a}{P_s} U_{P_s} \right)^2 \right]^{1/2} \tag{B.6}$$

Uncertainty of mass flow rate

The mass flow rate of mixture is

$$m_m = Q_l \rho_l + Q_g \rho_g = m_l + m_g \tag{B.7}$$

where ρ_g is the air density at standard conditions (1.2 kg/m^3) and ρ_l is density of oil (830kg/m^3).

Note of editor: Eq. (B.7) is incorrect. However, note the gas flowmeter displays the volumetric flow rate at standard conditions, hence the need to introduce ρ_g. The students do not know yet how to report this in an appropriate manner.

The uncertainty in the density of air and oil density is negligible, i.e., $U\rho_g$ and $U\rho_l \approx 0$. Hence, the relative uncertainty in mixture mass flow rate is

$$\frac{U_{m_m}}{m_m}=\left[\left(\frac{\partial m_m}{\partial Q_l}\frac{U_{Q_l}}{m_m}\right)^2+\left(\frac{\partial m_m}{\partial Q_g}\frac{U_{Q_g}}{m_m}\right)^2\right]^{\frac{1}{2}}=\left[\left(\frac{\rho_l}{m_m}U_{Q_l}\right)^2+\left(\frac{\rho_g}{m_m}U_{Q_g}\right)^2\right]^{\frac{1}{2}} \quad \text{(B.8)}$$

Table B.1 shows the uncertainty for the sensors and instruments used. Table B.2 shows the uncertainty of inlet LVF and mass flow rate calculated using equation (B.6) and (B.8).

Table B. 1. Uncertainty in flow rate and pressure measurements.

Variable	Manufacturer	Uncertainty
Supply pressure P_s [bar]	0.25%FS (full scale 200psia)	U_{PS} = ±0.5psi (±0.034bar)
Oil flow rate Q_l [L/min]	1%FS (full scale 5L/min)	U_{Ql} = ±0.05L/min
Air flow rate Q_g [SLPM]	1%FS (full scale 100SLPM)	U_{Qg} = ±1.0SLPM

Table B. 2. Uncertainty of seal inlet LVF and mixture mass flow rate. Test with *Ps*=3.5bar(a), *Pa*=1.0 bar(a), temperature ~20°C, stationary rotor.

Q_g SLPM	Q_l L/min	inlet LVF β_{inlet}	uncertainty in LVF -	m_m kg/s	uncertainty in m_m -
0	1.45	1.00	0	0.0200	3.5%
1.0	1.44	0.83	0.17	0.0199	3.5%
2.7	1.41	0.65	0.13	0.0196	3.5%
4.5	1.41	0.52	0.11	0.0196	3.5%
7.6	1.38	0.39	0.08	0.0193	3.6%
10.5	1.37	0.31	0.07	0.0192	3.6%
15.4	1.35	0.24	0.06	0.0190	3.6%
26	1.33	0.15	0.05	0.0189	3.7%
51	1.22	0.08	0.04	0.0178	3.9%
80	1.18	0.05	0.04	0.0178	3.9%
91	1.13	0.04	0.04	0.0175	4.0%

Initially, the uncertainty for β_{inlet} =0.83, 0.65, 0.52 is greater than 10%. This shortcoming is later solved by using a second air flow meter with a measuring range 0-5 L/min, and a with 1% measurement uncertainty. Later, the uncertainty for β_{inlet} =0.83, 0.65, 0.52 decreases to 1%, 1% and 2%, respectively.

Uncertainly of force coefficients

The test rig uses two Bently Nevada 3300 series eddy current sensors to measure the seal cartridge displacements with respect to a stationary journal. The calibrated sensitivity of the *X*- and *Y*- eddy current sensors is 7.64 V/mm and 8.07 V/mm. The DAQ system employs the I/O tech 652U to record the signal voltage, the amplitude accuracy of the I/O tech 625U for DC voltage is 0.2% of reading, thus renders the uncertainty for U_δ/δ=0.2% (U_δ/δ is the uncertainty of displacement and force caused by DQA system when convert the physical parameter into Voltage during the data acquiring process.)

The dynamic load cell sensitivities are 112 mV/N, and have non-linearity of 1% full scale, hence the relative uncertainty of the force is $U_F/F= (0.002^2+0.01^2)^{0.5}$ = 1%.

The resolution of frequency measurements is the ratio of the sampling rate to number of samples. The test sampling ratio is 12800 samples/s, the total sampling time is 0.64 s, rendering 8192 samples. The uncertainty in frequency is U_ω = 1.6 Hz. The relations to estimate the linearized force coefficients are [20]:

$$\begin{aligned} K &= \frac{\partial F}{\partial X} \rightarrow K \sim \frac{F}{X} \\ C &= \frac{\partial F}{\partial \dot{X}} \rightarrow C \sim \frac{F}{X\omega} \\ M &= \frac{\partial F}{\partial \ddot{X}} \rightarrow M \sim \frac{F}{X\omega^2} \end{aligned} \qquad \text{(B.9)}$$

where *F* and *X* are the applied dynamic force and ensuing displacement, and (*K, C, M*) are force coefficeints derived from a test at frequency ω. The relative uncertainty for the parameters is:

$$\begin{aligned} \frac{U_K}{K} &= \sqrt{\left(\frac{U_F}{F}\right)^2 + \left(\frac{U_X}{X}\right)^2} \\ \frac{U_C}{C} &= \sqrt{\left(\frac{U_F}{F}\right)^2 + \left(\frac{U_X}{X}\right)^2 + \left(\frac{U_\omega}{\omega}\right)^2} \\ \frac{U_M}{M} &= \sqrt{\left(\frac{U_F}{F}\right)^2 + \left(\frac{U_X}{X}\right)^2 + 2\left(\frac{U_\omega}{\omega}\right)^2} \end{aligned} \qquad \text{(B.10)}$$

Note of editor: the analysis above is overly simplistic, as the procedure considers a MISO (multiple input, single output) identification. Please note that the parameters are related to each other and a function of the excitation frequency.

Since the displacement sensors are calibrated with a dial gauge with accuracy 0.001 mm, the displacement amplitude for dynamic test is ~1 mil, the uncertainty for displacement is U_X/X =1/25.4≈0.04. The test external excitation force has frequency from 30 HZ to 250 HZ. Substituting the displacement measurement uncertainty and force measurement uncertainty into (B.10), one obtains the uncertainty of the stiffness. Then the

equation (B.10) also propagates the uncertainty of the damping coefficient and mass coefficients shown in Table B.3.

Table B. 3. Uncertainty of estimated physical parameters for test seal

Uncertainty	Test Frequency	
	30 Hz	250 Hz
U_K/K	4.1%	4.1%
U_C/C	6.6%	4.2%
U_M/M	8.5%	4.2%

Note of editor: The uncertainty analysis addresses to the precision of the instruments only. It does not consider the variability in results from one test to the next, as well as the variations due to changes in operating conditions. The reader must exercise caution when considering the results above. Later, a more detailed analysis will be conducted.

Appendix C. Real & Imaginary Parts of Cross-Coupled H_{XY} and H_{YX} for *Wet Seal*

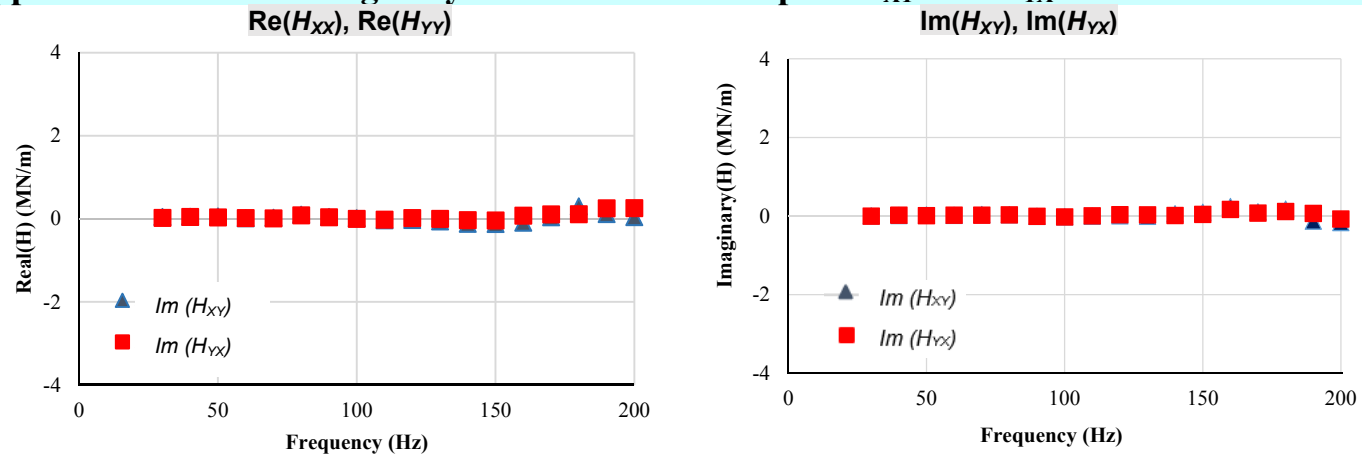

(a) β_{inlet} = 0, all gas (m_m=6±0.8 g/s)

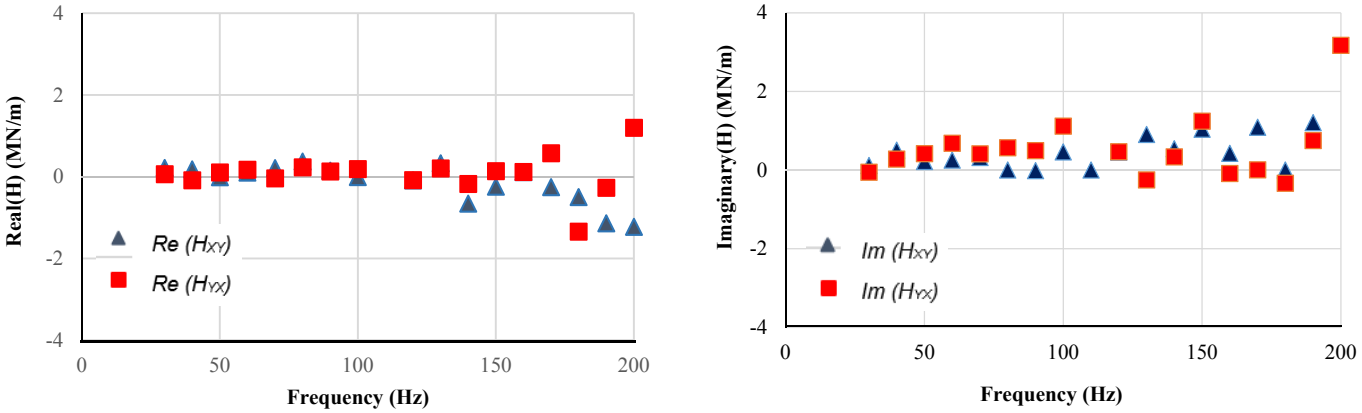

(b) β_{inlet} = 0.02, λ=0.90 (m_m=6±0.2 g/s)

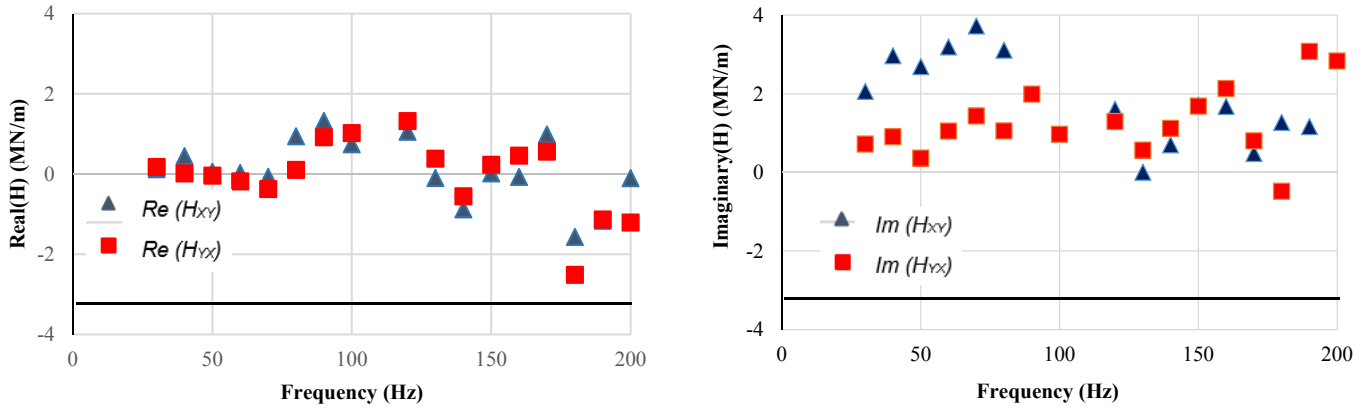

(c) β_{inlet} = 0.04, λ= 0.95 (m_m=7±0.2 g/s)

Figure C.1. Real and imaginary parts of cross-coupled complex stiffnesses (H_{XY}, H_{YX}) for *wet seal* supplied with an oil in air mixture with inlet LVF (a) 0% (all gas), (b) 2%, and (c) 4%. Stationary (non-rotating) journal. Tests with supply pressure P_S=2.0 bar(abs), ambient pressure P_a=1 bar(abs), inlet temperature 20°C.

Appendix D. Oil Viscosity Measurement

Error! Reference source not found.D.1 and **Error! Reference source not found.**D.1 show the viscosity vs temperature for the ISO-VG10 oil as recorded on different dates from November 2014 to January 2015. The results show the oil remains the same after months of multiple tests.

Table D. 1. ISO VG 10 – oil viscosity vs. temperature (two dates)

Date: 11/19/2014		Date: 01/24/2015	
Temp(˚C)	Viscosity (cP)	Temp(˚C)	Viscosity (cP)
19.6	18.42	20.1	18.21
20.6	17.64	21	17.55
21.2	17.25	21.4	17.28
22.2	16.56	22.6	16.47
23.1	16.05	23.4	15.96
24	15.48	24.8	15.09
25.1	14.88	25.1	14.94
27	13.8	27	13.92
30	12.39	30	12.51
35	10.47	35	10.62
40	8.94	40	9.09
50	6.78	50	6.84

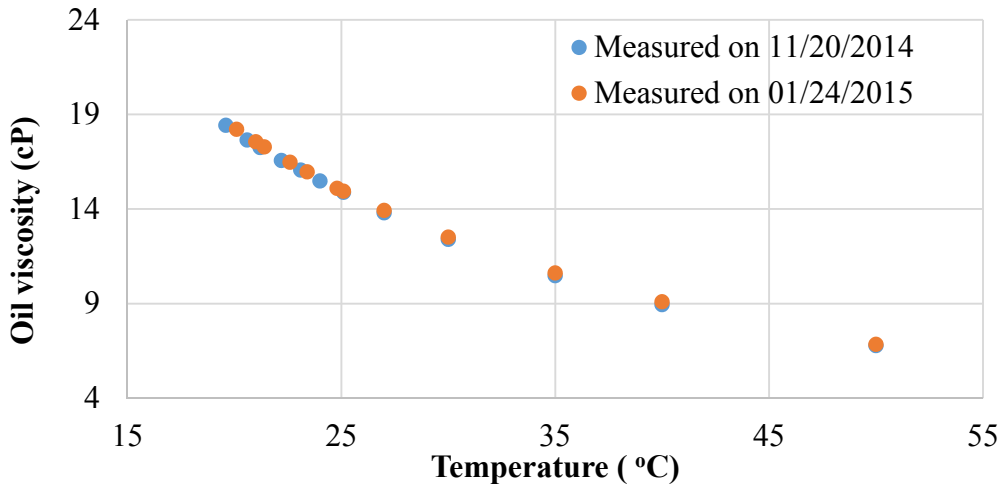

Figure D. 1. Lubricant viscosity versus temperature. Measurements on two dates.